How to cite: *Angew. Chem. Int. Ed.* **2021**, *60*, 17910–17914
International Edition: doi.org/10.1002/anie.202105032
German Edition: doi.org/10.1002/ange.202105032

Fluorescence

Hypsochromic Shift of Multiple-Resonance-Induced Thermally Activated Delayed Fluorescence by Oxygen Atom Incorporation

*Hiroyuki Tanaka, Susumu Oda, Gaetano Ricci, Hajime Gotoh, Keita Tabata, Ryosuke Kawasumi, David Beljonne, Yoann Olivier, and Takuji Hatakeyama**

Abstract: *Herein, we reported an ultrapure blue multiple-resonance-induced thermally activated delayed fluorescence (MR-TADF) material (**ν-DABNA-O-Me**) with a high photoluminescence quantum yield and a large rate constant for reverse intersystem crossing. Because of restricted π-conjugation of the HOMO rather than the LUMO induced by oxygen atom incorporation, **ν-DABNA-O-Me** shows a hypsochromic shift compared to the parent MR-TADF material (**ν-DABNA**). An organic light-emitting diode based on this material exhibits an emission at 465 nm, with a small full-width at half-maximum of 23 nm and Commission Internationale de l'Eclairage coordinates of (0.13, 0.10), and a high maximum external quantum efficiency of 29.5 %. Moreover, **ν-DABNA-O-Me** facilitates a drastically improved efficiency roll-off and a device lifetime compared to **ν-DABNA**, which demonstrates significant potential of the oxygen atom incorporation strategy.*

Recently, thermally activated delayed fluorescence (TADF) materials[1] have garnered significant attention as efficient emitters for application in organic light-emitting diodes (OLEDs).[2] This can be attributed to their expected internal quantum efficiency (IQE) of 100 % without employing precious metals. In such systems, a small singlet–triplet energy gap (ΔE_{ST}) is necessary to facilitate upconversion from the non-radiative lowest triplet excited state (T_1) to the radiative lowest singlet excited state (S_1) through reverse intersystem crossing (RISC). The most common strategy to attain a small ΔE_{ST} involves the separation of the highest occupied molecular orbital (HOMO) and lowest occupied molecular orbital (LUMO) through the introduction of donor and acceptor groups.[3] However, donor-acceptor (D-A) type TADF materials display large Stokes shifts and broadened emission spectra owing to structural relaxation in the excited states. The typical full widths at half-maxima (FWHMs) are above 70 nm, which hampers the practical applications of TADF materials in OLED displays.

We previously reported an alternative strategy to separate HOMO and LUMO, aimed at overcoming the aforementioned shortcomings. The reported strategy was based on the multiple resonance (MR) effect of boron and nitrogen atoms. For the first time, this strategy was employed to develop **DABNA-1** as a pure-blue TADF emitter.[4] In the molecule, the LUMOs and HOMOs are localized on the *ortho* and *para* positions of the boron and nitrogen atoms, respectively. The MR-based HOMO/LUMO separation resulted in a low ΔE_{ST} of < 0.20 eV; furthermore, a high photoluminescence quantum yield (PLQY) and narrowband emission with an FWHM of < 30 nm was obtained. This was attributed to the suppressed vibronic coupling between the S_0 and S_1 states.[5] Owing to the favorable properties of **DABNA-1**, a number of MR-TADF materials,[6,7] were developed by introducing a ring-fused structure[8] or appropriate substituents.[9] However, these materials exhibited a relatively small RISC rate constant (k_{RISC}; ca. 10^4 s^{-1}), which can lead to efficiency roll-off at high luminance intensities. Moreover, all the modifications are accompanied by a bathochromic shift due to the extension of the π-conjugation, and deep blue emission cannot be realized. Recently, we developed a new MR-TADF **ν-DABNA**[10] with a fully resonating extended π-skeleton (Figure 1). Because of the CT delocalization,[11] **ν-DABNA** exhibited a significantly higher k_{RISC} (2.0×10^5 s^{-1}) and realized an OLED exhibiting an excellent external quantum efficiency (EQE) with a minimum efficiency roll-off (34.4 %/32.8 %/26.0 % at 15/100/1000 cd m^{-2}, respectively). Furthermore, the alternating localization of the HOMO–LUMO suppressed the vibronic coupling between the S_0 and S_1 states to exhibit an unprecedented sharp electroluminescence (EL) emission with an FWHM of 18 nm. However, the emission maximum of **ν-DABNA** was 469 nm, which was slightly red-shifted from that of **DABNA-1** (459 nm) because of the π-extension. As a result, the Commission Internationale de l'Eclairage (CIE) coordinates (0.12, 0.11) were deviated from the requirements defined by the National Television System Committee (0.14, 0.08). Herein, we propose a novel MR-TADF material (**ν-DABNA-O**) possessing an oxygen atom instead of a nitrogen atom (Figure 1). Because of its lower atomic orbital energy, the oxygen atom restricts π-conjugation of the HOMO rather than the LUMO. This leads to a larger deviation in the HOMO energy level (−0.16 eV) than

[*] H. Tanaka, Dr. S. Oda, H. Gotoh, K. Tabata, Prof. T. Hatakeyama
Department of Chemistry, School of Science and Technology, Kwansei Gakuin University
2-1 Gakuen, Sanda, Hyogo 669-1337 (Japan)
E-mail: hatake@kwansei.ac.jp
H. Tanaka, K. Tabata, R. Kawasumi
JNC Petrochemical Corporation
5-1 Goi Kaigan, Ichihara, Chiba 290-8551 (Japan)
G. Ricci, Prof. Y. Olivier
Unité de Chimie Physique Théorique et Structurale & Laboratoire de Physique du Solide, Namur Institute of Structured Matter
Université de Namur
Rue de Bruxelles, 61, 5000 Namur (Belgium)
Dr. D. Beljonne
Laboratory for Chemistry of Novel Materials, Université de Mons
Place du Parc 20, 7000 Mons (Belgium)
Supporting information and the ORCID identification number(s) for the author(s) of this article can be found under: https://doi.org/10.1002/anie.202105032.

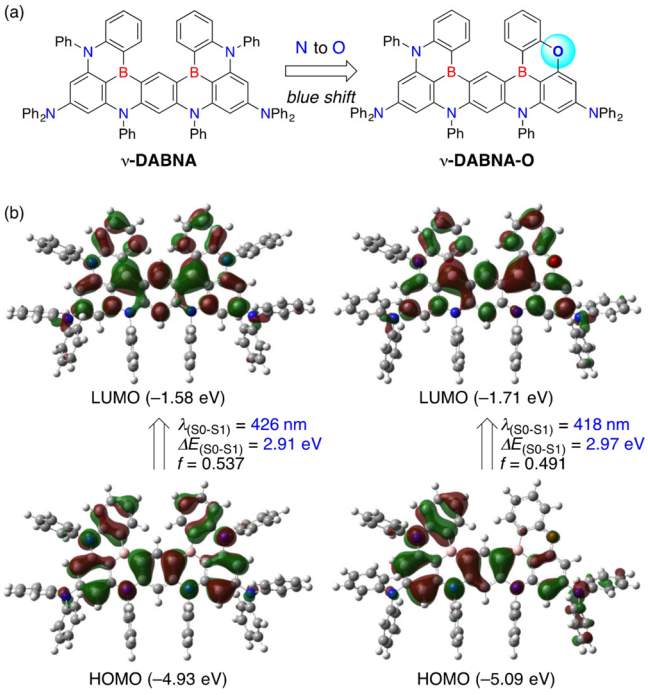

Figure 1. a) Design of MR-TADF materials by the oxygen atom incorporation. b) Kohn–Sham frontier orbitals of **ν-DABNA** and **ν-DABNA-O** calculated at the B3LYP/6–311 + G(d,p) level of theory. and the oscillator strength (*f*) and S_0-S_1 transition energy (ΔE, λ) at the ADC(2)/def2-SVP//B3LYP/6–311 + G(d,p) level of theory.

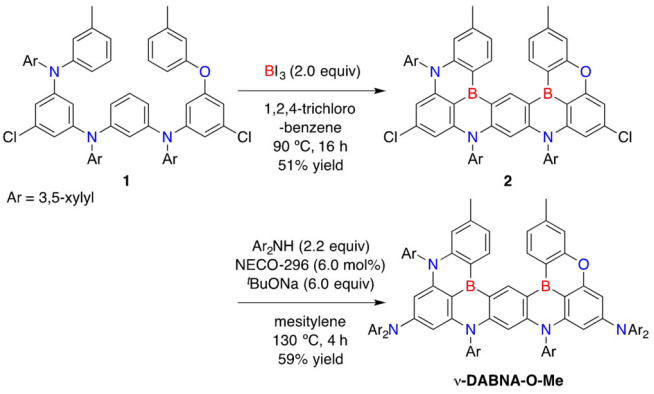

Figure 2. Synthesis of **ν-DABNA-O-Me**.

the LUMO energy level (–0.13 eV). As a result, **ν-DABNA-O** exhibits a larger HOMO–LUMO gap and is consequently expected to display a deeper blue emission than **ν-DABNA**.

The synthesis of **ν-DABNA-O** is summarized in Figure 2. We aimed to construct the core skeleton via one-shot borylation;[7,10] therefore, methyl and chlorine groups were introduced to suppress the undesired borylation reactions. Precursor **1** was synthesized in four steps from commercially available starting materials (Supporting Information, Scheme S1). The one-shot double borylation of **1** was carried out with a stoichiometric amount of BI_3[7,12] at 90 °C to obtain a 51 % yield of intermediate **2**. In the presence of a catalytic amount of bis(di-*tert*-butyl(3-methyl-2-butenyl)phosphine)dichloro palladium (NECO-296), cross-coupling reaction with bis(3,5-dimethylphenyl)amine took place at 130 °C to result in a 59 % yield of **ν-DABNA-O-Me**. These processes are scalable and suitable for structural modification by introducing various substituents to adjust the photophysical properties for a variety of applications.

The photophysical properties of **ν-DABNA-O-Me** in the form of a thin film (1 wt % doped in polymethyl methacrylate (PMMA)) are presented in Figure 3. The ultraviolet (UV)-visible absorption spectrum revealed a strong absorption band corresponding to the HOMO–LUMO transition, with a maximum at 449 nm (Figure 3 a). The fluorescence spectrum at 300 K revealed a strong and sharp deep-blue emission band at 464 nm (Figure 3 a), which is blue-shifted by 5 nm from that of **ν-DABNA**.[10] The Stokes shift and FWHM were exceedingly small (15 and 24 nm, respectively), indicating that the non-bonding HOMO and LUMO minimize the vibronic coupling between the S_1-S_0 transition and stretching/scissoring vibrations. To determine ΔE_{ST}, we recorded the emission spectra of the **ν-DABNA-O-Me** film at 77 K with and without delay (Figure 3 b). At a delay of 25 ms, the emission maximum was red-shifted by 22 nm (i.e., from 466 to 488 nm), which was attributed to phosphorescence. Based on the emission maximum of each spectrum, ΔE_{ST} was estimated to be 29 meV

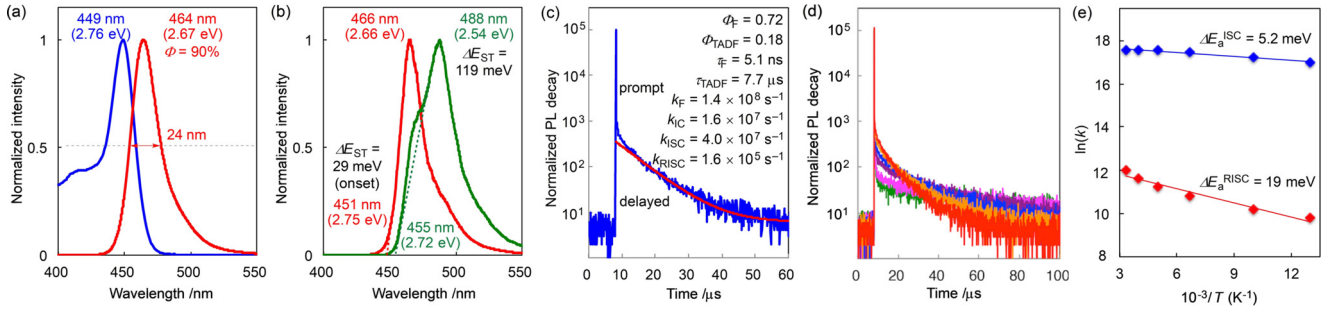

Figure 3. Photophysical properties of **ν-DABNA-O-Me** in PMMA (1 wt %-doped film). a) Absorption (blue) and fluorescence (red) spectra at 300 K. b) Fluorescence spectra at 77 K with (green)/without (red) a delay time of 25 ms. c) Transient decay spectrum at 300 K and its associated photophysical properties. The red curve represents the single exponential fit of the data with a background of 5. Φ_F (Φ_{TADF}) and τ_F (τ_{TADF}): quantum yield and lifetime of fluorescent (TADF) components, respectively; k_F, k_{IC}, k_{ISC}, and k_{RISC}: rate constants of fluorescence, internal conversion, intersystem crossing, and reverse intersystem crossing, respectively. d) Transient decay spectra at 77 (green), 100 (magenta), 150 (purple), 200 (blue), 250 (orange), and 300 K (red). e) Arrhenius plot of k_{RISC} and k_{ISC} vs. $1/T$.

from onset (119 meV from peak top), larger than that of **ν-DABNA** (18 meV).[14] This trend is in excellent agreement with the ΔE_{ST} computed by the second-order algebraic diagrammatic construction (ADC(2)) method, which amounts to 42 meV and 55 meV for **ν-DABNA** and **ν-DABNA-O-Me**, respectively.[14] In addition, the transient spectrum of the film was measured to evaluate the TADF properties (Figure 3c). Based on the quantum yields (Φ_F = 0.72 and Φ_{TADF} = 0.18) and lifetimes (τ_F = 5.1 ns and τ_{TADF} = 7.7 μs) of the fluorescence (prompt) and TADF (delayed) components, the rate constants for fluorescence (k_F), internal conversion (k_{IC}), intersystem crossing (k_{ISC}), and reverse intersystem (k_{RISC}) were calculated to be 1.4×10^8, 1.6×10^7, 4.0×10^7, and 1.6×10^5 s^{-1}, respectively, using a method provided in the literature.[13] Notably, **ν-DABNA-O-Me** exhibited a k_{RISC} value that was comparable to that of **ν-DABNA** (2.0×10^5 s^{-1}). The increase in ΔE_{ST} of **ν-DABNA-O-Me** with respect to **ν-DABNA** comes along with an increase in spin-orbit coupling (SOC), as computed from TD-DFT calculations within the Tamm-Dancoff approximation using the PBE0 functional and the double zeta polarized basis set[14] ($\langle S_1|\hat{H}_{SO}|T_n\rangle$ of **ν-DABNA**: T_1: 0.028 cm^{-1}; T_2: 0.051 cm^{-1}, **ν-DABNA-O-Me**: T_1: 0.032 cm^{-1}; T_2: 0.054 cm^{-1}, respectively), which give rise to the comparable k_{RISC} values ($\propto \langle S_1|\hat{H}_{SO}|T_n\rangle^2$ and $\exp(-\Delta E_{ST})$).[15] Moreover, the $\Delta E_{T_2\text{-}S_1}$ of **ν-DABNA-O-Me** computed to by the ADC(2) method is smaller than that of **ν-DABNA** (59 meV and 80 meV, respectively),[14] suggesting significant contribution of T_2 to the RISC process. The increase in $\langle S_1|\hat{H}_{SO}|T_n\rangle$ of **ν-DABNA-O-Me** with respect to **ν-DABNA** is confirmed to be due to the larger difference in the nature of the S_1 and T_n excited states[14] in line with El-Sayed rules.

The transient spectra at different temperatures (from 77 to 300 K) are shown in Figure 3d. The TADF component decreases at lower temperatures, but remains conspicuous at 77 K. From the Arrhenius plots of k_{RISC} vs. $1/T$,[1a] the RISC and ISC activation energies (ΔE_a^{RISC}, ΔE_a^{ISC}) were estimated to be 19 and 5.2 meV, respectively, which are lower than those of **ν-DABNA** (ΔE_a^{RISC} = 70 meV), thereby aiding the mitigation of the temperature dependency of device performance. Low reorganization energies between T_n and S_1 states (λ = 17 and 69 meV for T_1 and T_2, respectively)[14] can account for the low activation energy.[15]

To demonstrate the potential of the proposed emitter, devices with the following structure were fabricated: indium tin oxide (ITO, 50 nm); *N*,*N*′-di(1-naphthyl)-*N*,*N*′-diphenyl-(1,1′-biphenyl)-4,4′-diamine (**NPD**, 40 nm); tris(4-carbazolyl-9-ylphenyl)amine (**TCTA**, 15 nm); 1,3-bis(*N*-carbazolyl)benzene (**mCP**, 15 nm); 1 wt% **ν-DABNA-O-Me** emitter and 99 wt% **DOBNA-Tol**[8e,16a] (20 nm); 3,4-di(9H-carbazol-9-yl)benzonitrile (**3,4-2CzBN**,[16b] 10 nm); 2,7-bis(2,2′-bipyridine-5-yl)triphenylene (**BPy-TP2**,[16c] 20 nm); LiF (1 nm); and Al (100 nm). The EL characteristics, ionization potentials, and electron affinities of the device are shown in Figure 4. The device exhibits a pure blue emission at 465 nm with an FWHM of 23 nm; the corresponding CIE coordinates are (0.13, 0.10), approaching the (0.14, 0.08) requirements defined by the National Television System Committee. Furthermore, the device exhibits excellent efficiencies of 29.5% at the maximum (1 cd m^{-2}), 29.1% at 10 cd m^{-2}, 28.8% at 100 cd m^{-2}, and 26.9% at 1000 cd m^{-2}. Notably, the efficiency roll-off of the device with **ν-DABNA-O-Me** (0.4%, 0.7%, and 2.6% at 10, 100, and 1000 cd m^{-2}, respectively) is lower than that with **ν-DABNA** (8.4% at 1000 cd m^{-2})[10] and those observed for the recently reported deep-blue OLEDs.[1c,e,i,4,7,17] We assume that the relatively high k_{RISC} value (1.6×10^5 s^{-1}) and balanced carrier injection suppress the triplet-triplet[18] and triplet-polaron annihilation

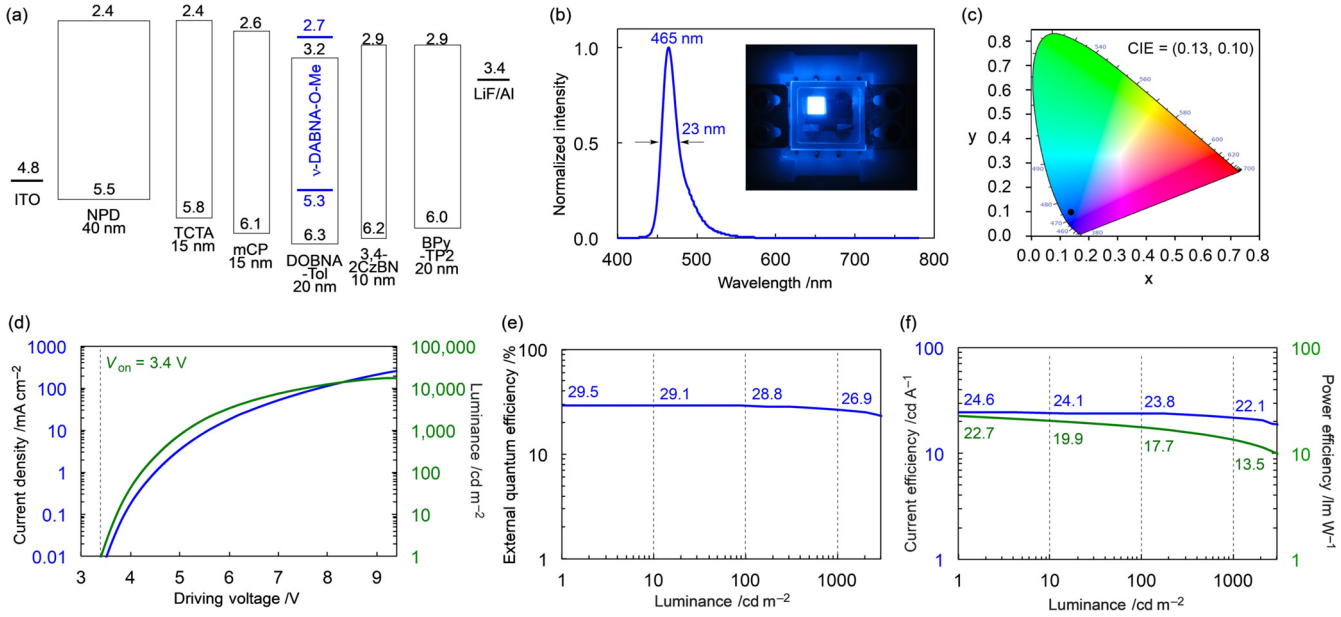

Figure 4. OLED performance. a) Device structure, ionization potentials, and electron affinities (in eV) for each component. b) Normalized EL spectra of the device in operation. Inset: electroluminescence of the device. c) CIE(*x*,*y*) coordinates. d) Current density (blue) and luminance (green) vs. driving voltage. e) EQE vs. luminance. f) Current (blue) and power efficiency (green) vs. luminance.

processes in the device. Notably, the device lifetime with **ν-DABNA-O-Me** is 10 times longer than that with **ν-DABNA** ($LT_{50} = 314$ and 31 h at 100 cd m^{-2}, respectively),[10] which can be ascribed to the use of **3,4-2CzBN** and **DOBNA-Tol** instead of **TSPO1** and **DOBNA-OAr**, respectively. Although this is insufficient for practical use, further improvement can be realized through the structural modification of **ν-DABNA-O-Me** and the optimization of the device structure using an assist dopant[19] or exciplex host system.[20]

In conclusion, in this study, we designed and synthesized an ultrapure deep-blue MR-TADF emitter (**ν-DABNA-O-Me**) with a high quantum yield, a short TADF lifetime, and a high k_{RISC} value. The OLED employing the **ν-DABNA-O-Me** as the emitter exhibited an emission at 465 nm with an FWHM of 23 nm, CIE coordinates of (0.13, 0.10), and a maximum EQE of 29.5%, which is the record-setting performance of blue TADF-OLEDs. Moreover, the device provided considerably lower efficiency roll-off and longer device lifetime than those with **ν-DABNA**. The proposed oxygen-atom-incorporation strategy for inducing the hypsochromic shift of the emission will pave the way for further refinement and development of MR-TADF materials.

Acknowledgements

This study was supported by Grant-in-Aid for Scientific Research (18H02051, 21H02019), Early-Career Scientists (20K15291), and Transformative Research Areas (Condensed Conjugation, 20H05863) from JSPS, CREST (JPMJCR18R3) programs from JST, the Asahi Glass Foundation, and the Nagase Science and Technology Foundation. The authors are grateful to H. Nishi, K. Yoshiura (Kwansei Gakuin University), Y. Kondo. Dr. T. Matsushita, Dr. K. Okumura, Dr. Y. Sasada, and Dr. M. Kondo (JNC Petrochemical Co.) for their support and valuable input. Computational resources were provided by the "Consortium des'Equipements de Calcul Intensif" (CÉCI), funded by the "Fonds de la Recherche Scientifiques de Belgique" (FRS-FNRS) under Grant No. 2.5020.11, as well as the Tier-1 supercomputer of the Fédération Wallonie-Bruxelles, infrastructure funded by the Walloon Region under Grant Agreement n1117545, and FRS-FNRS. Y.O. acknowledges funding from the FRS-FNRS under the grant F.4534.21 (MIS-IMAGINE). G.R. acknowledges a grant from the "Fonds pour la formation a la Recherche dans l'Industrie et dans l'Agriculture" (FRIA) of the FRS-FNRS.

Conflict of interest

The authors declare no conflict of interest.

Keywords: deep blue · multiple resonance effect · narrowband emission · organic light-emitting diodes · thermally activated delayed fluorescence

[1] a) H. Uoyama, K. Goushi, K. Shizu, H. Nomura, C. Adachi, *Nature* **2012**, *492*, 234; b) F. B. Dias, K. N. Bourdakos, V. Jankus, K. C. Moss, K. T. Kamtekar, V. Bhalla, J. Santos, M. R. Bryce, A. P. Monkman, *Adv. Mater.* **2013**, *25*, 3707; c) Q. Zhang, B. Li, S. Huang, H. Nomura, H. Tanaka, C. Adachi, *Nat. Photonics* **2014**, *8*, 326; d) H. Wang, L. Xie, Q. Peng, L. Meng, Y. Wang, Y. Yi, P. Wang, *Adv. Mater.* **2014**, *26*, 5198; e) S. Hirata, Y. Sakai, K. Masui, H. Tanaka, S. Y. Lee, H. Nomura, N. Nakamura, M. Yasumatsu, H. Nakanotani, Q. Zhang, K. Shizu, H. Miyazaki, C. Adachi, *Nat. Mater.* **2015**, *14*, 330; f) K. Suzuki, S. Kubo, K. Shizu, T. Fukushima, A. Wakamiya, Y. Murata, C. Adachi, H. Kaji, *Angew. Chem. Int. Ed.* **2015**, *54*, 15231; *Angew. Chem.* **2015**, *127*, 15446; g) P. Data, P. Pander, M. Okazaki, Y. Takeda, S. Minakata, A. P. Monkman, *Angew. Chem. Int. Ed.* **2016**, *55*, 5739; *Angew. Chem.* **2016**, *128*, 5833; h) Y. Seino, S. Inomata, H. Sasabe, Y.-J. Pu, J. Kido, *Adv. Mater.* **2016**, *28*, 2638; i) I. S. Park, K. Matsuo, N. Aizawa, T. Yasuda, *Adv. Funct. Mater.* **2018**, *28*, 1802031; j) T.-L. Wu, M.-J. Huang, C.-C. Lin, P.-Y. Huang, T.-Y. Chou, R.-W. Chen-Cheng, H.-W. Lin, R.-S. Liu, C.-H. Cheng, *Nat. Photonics* **2018**, *12*, 23.

[2] C. W. Tang, S. A. VanSlyke, *Appl. Phys. Lett.* **1987**, *51*, 913.

[3] Reviews: a) Y. Im, M. Kim, Y. J. Cho, J.-A. Seo, K. S. Yook, J. Y. Lee, *Chem. Mater.* **2017**, *29*, 1946; b) Z. Yang, Z. Mao, Z. Xie, Y. Zhang, S. Liu, J. Zhao, J. Xu, Z. Chi, M. P. Aldred, *Chem. Soc. Rev.* **2017**, *46*, 915; c) M. Y. Wong, E. Zysman-Colman, *Adv. Mater.* **2017**, *29*, 1605444; d) X. Cai, S.-J. Su, *Adv. Funct. Mater.* **2018**, *28*, 1802558.

[4] T. Hatakeyama, K. Shiren, K. Nakajima, S. Nomura, S. Nakatsuka, K. Kinoshita, J. Ni, Y. Ono, T. Ikuta, *Adv. Mater.* **2016**, *28*, 2777.

[5] a) D. S. Karpovich, G. J. Blanchard, *J. Phys. Chem.* **1995**, *99*, 3951; b) F. Santoro, A. Lami, R. Improta, J. Bloino, V. Barone, *J. Chem. Phys.* **2008**, *128*, 224311; c) T. Sato, K. Tokunaga, N. Iwahara, K. Shizu, K. Tanaka, *The Jahn–Teller Effect: Fundamentals and Implications for Physics and Chemistry*, Springer Series in Chemical Physics, *Vol. 97*, Springer, Heidelberg, **2009**, pp. 99–129; d) M. Uejima, T. Sato, D. Yokoyama, K. Tanaka, J.-W. Park, *Phys. Chem. Chem. Phys.* **2014**, *16*, 14244; e) T. Xiong, W. Włodarczyk, P. Saalfrank, *Chem. Phys.* **2018**, *515*, 728.

[6] a) S. Madayanad Suresh, D. Hall, D. Beljonne, Y. Olivier, E. Zysman-Colman, *Adv. Funct. Mater.* **2020**, *30*, 1908677; b) S. M. Suresh, E. Duda, D. Hall, Z. Yao, S. Bagnich, A. M. Z. Slawin, H. Bässler, D. Beljonne, M. Buck, Y. Olivier, A. Köhler, E. Zysman-Colman, *J. Am. Chem. Soc.* **2020**, *142*, 6588.

[7] a) K. Matsui, S. Oda, K. Yoshiura, K. Nakajima, N. Yasuda, T. Hatakeyama, *J. Am. Chem. Soc.* **2018**, *140*, 1195; b) S. Oda, B. Kawakami, R. Kawasumi, R. Okita, T. Hatakeyama, *Org. Lett.* **2019**, *21*, 9311; c) N. Ikeda, S. Oda, R. Matsumoto, M. Yoshioka, D. Fukushima, K. Yoshiura, N. Yasuda, T. Hatakeyama, *Adv. Mater.* **2020**, *32*, 2004072.

[8] a) Y. Zhang, D. Zhang, J. Wei, Z. Liu, Y. Lu, L. Duan, *Angew. Chem. Int. Ed.* **2019**, *58*, 16912; *Angew. Chem.* **2019**, *131*, 17068; b) Y. Xu, C. Li, Z. Li, Q. Wang, X. Cai, J. Wei, Y. Wang, *Angew. Chem. Int. Ed.* **2020**, *59*, 17442; *Angew. Chem.* **2020**, *132*, 17595; c) Y. Zhang, D. Zhang, J. Wei, X. Hong, Y. Lu, D. Hu, G. Li, Z. Liu, Y. Chen, L. Duan, *Angew. Chem. Int. Ed.* **2020**, *59*, 17499; *Angew. Chem.* **2020**, *132*, 17652; d) M. Yang, I. S. Park, T. Yasuda, *J. Am. Chem. Soc.* **2020**, *142*, 19468; e) S. Oda, W. Kumano, T. Hama, R. Kawasumi, K. Yoshiura, T. Hatakeyama, *Angew. Chem. Int. Ed.* **2021**, *60*, 2882; *Angew. Chem.* **2021**, *133*, 2918.

[9] a) X. Liang, Z.-P. Yan, H.-B. Han, Z.-G. Wu, Y.-X. Zheng, H. Meng, J.-L. Zuo, W. Huang, *Angew. Chem. Int. Ed.* **2018**, *57*, 11316; *Angew. Chem.* **2018**, *130*, 11486; b) S. H. Han, J. H. Jeong, J. W. Yoo, J. Y. Lee, *J. Mater. Chem. C* **2019**, *7*, 3082.

[10] Y. Kondo, K. Yoshiura, S. Kitera, H. Nishi, S. Oda, H. Gotoh, Y. Sasada, M. Yanai, T. Hatakeyama, *Nat. Photonics* **2019**, *13*, 678.
[11] A. Pershin, D. Hall, V. Lemaur, J.-C. Sancho-Garcia, L. Muccioli, E. Zysman-Colman, D. Beljonne, Y. Olivier, *Nat. Commun.* **2019**, *10*, 597.
[12] a) S. Oda, K. Ueura, B. Kawakami, T. Hatakeyama, *Org. Lett.* **2020**, *22*, 700; b) S. Oda, T. Hatakeyama, *Bull. Chem. Soc. Jpn.* **2021**, *94*, 950.
[13] a) Q. Zhang, H. Kuwabara, W. J. Potscavage, Jr., S. Huang, Y. Hatae, T. Shibata, C. Adachi, *J. Am. Chem. Soc.* **2014**, *136*, 18070; b) H. Kaji, H. Suzuki, T. Fukushima, K. Shizu, K. Katsuaki, S. Kubo, T. Komino, H. Oiwa, F. Suzuki, A. Wakamiya, Y. Murata, C. Adachi, *Nat. Commun.* **2015**, *6*, 8476.
[14] See the supporting information for details.
[15] a) J. Gibson, A. P. Monkman, T. J. Penfold, *ChemPhysChem* **2016**, *17*, 2956; b) M. K. Etherington, J. Gibson, H. F. Higginbotham, T. J. Penfold, A. P. Monkman, *Nat. Commun.* **2016**, *7*, 13680; c) P. K. Samanta, D. Kim, V. Coropceanu, J.-L. Brédas, *J. Am. Chem. Soc.* **2017**, *139*, 4042; d) H. Noda, X.-K. Chen, H. Nakanotani, T. Hosokai, M. Miyajima, N. Notsuka, Y. Kashima, J.-L. Brédas, C. Adachi, *Nat. Mater.* **2019**, *18*, 1084; e) N. Aizawa, Y. Harabuchi, S. Maeda, Y.-J. Pu, *Nat. Commun.* **2020**, *11*, 3909.
[16] a) H. Hirai, K. Nakajima, S. Nakatsuka, K. Shiren, J. Ni, S. Nomura, T. Ikuta, T. Hatakeyama, *Angew. Chem. Int. Ed.* **2015**, *54*, 13581; *Angew. Chem.* **2015**, *127*, 13785; b) K. Togashi, S. Nomura, N. Yokoyama, T. Yasuda, C. Adachi, *J. Mater. Chem.* **2012**, *22*, 20689; c) Y. Tanaka, T. Takahashi, J. Nishide, Y. Hiraga, H. Nakanotani, C. Adachi, *Thin Solid Films* **2016**, *619*, 120.
[17] a) T.-A. Lin, T. Chatterjee, W.-L. Tsai, W.-K. Lee, M.-J. Wu, M. Jiao, K.-C. Pan, C.-L. Yi, C.-L. Chung, K.-T. Wong, C.-C. Wu, *Adv. Mater.* **2016**, *28*, 6976; b) Y. Li, X.-L. Li, D. Chen, X. Cai, G. Xie, Z. He, Y.-C. Wu, A. Lien, Y. Cao, S.-J. Su, *Adv. Funct. Mater.* **2016**, *26*, 6904; c) H. Tsujimoto, D.-G. Ha, G. Markopoulos, H. S. Chae, M. A. Baldo, T. M. Swager, *J. Am. Chem. Soc.* **2017**, *139*, 4894; d) P. Rajamalli, N. Senthilkumar, P.-Y. Huang, C.-C. Ren-Wu, H.-W. Lin, C.-H. Cheng, *J. Am. Chem. Soc.* **2017**, *139*, 10948; e) S. Shao, J. Hu, X. Wang, L. Wang, X. Jing, F. Wang, *J. Am. Chem. Soc.* **2017**, *139*, 17739; f) L.-S. Cui, H. Nomura, Y. Geng, J. Y. Kim, H. Nakanotani, C. Adachi, *Angew. Chem. Int. Ed.* **2017**, *56*, 1571; *Angew. Chem.* **2017**, *129*, 1593; g) Y. Wada, S. Kubo, H. Kaji, *Adv. Mater.* **2018**, *30*, 1705641; h) K. Matsuo, T. Yasuda, *Chem. Sci.* **2019**, *10*, 10687; i) S.-J. Zou, F.-M. Xie, M. Xie, Y.-Q. Li, T. Cheng, X.-H. Zhang, C.-S. Lee, J.-X. Tang, *Adv. Sci.* **2020**, *7*, 1902508; j) J. U. Kim, I. S. Park, C.-Y. Chan, M. Tanaka, Y. Tsuchiya, H. Nakanotani, C. Adachi, *Nat. Commun.* **2020**, *11*, 1765; k) T. Agou, K. Matsuo, R. Kawano, I. S. Park, T. Hosoya, H. Fukumoto, T. Kubota, Y. Mizuhata, N. Tokitoh, T. Yasuda, *ACS Mater. Lett.* **2020**, *2*, 28.
[18] C. Xiang, X. Fu, W. Wei, R. Liu, Y. Zhang, V. Balema, B. Nelson, F. So, *Adv. Funct. Mater.* **2016**, *26*, 1463.
[19] a) H. Nakanotani, T. Higuchi, T. Furukawa, K. Masui, K. Morimoto, M. Numata, H. Tanaka, Y. Sagara, T. Yasuda, C. Adachi, *Nat. Commun.* **2014**, *5*, 4016; b) D. Zhang, X. Song, A. J. Gillett, B. H. Drummond, S. T. E. Jones, G. Li, H. He, M. Cai, D. Credgington, L. Duan, *Adv. Mater.* **2020**, *32*, 1908355; c) C.-Y. Chan, M. Tanaka, Y.-T. Lee, Y.-W. Wong, H. Nakanotani, T. Hatakeyama, C. Adachi, *Nat. Photonics* **2021**, *15*, 203; d) S. O. Jeon, K. H. Lee, J. S. Kim, S.-G. Ihn, Y. S. Chung, J. W. Kim, H. Lee, S. Kim, H. Choi, J. Y. Lee, *Nat. Photonics* **2021**, *15*, 208.
[20] T. B. Nguyen, H. Nakanotani, T. Hatakeyama, C. Adachi, *Adv. Mater.* **2020**, *32*, 1906614.

Manuscript received: April 12, 2021
Revised manuscript received: May 15, 2021
Accepted manuscript online: May 26, 2021
Version of record online: July 2, 2021

